Crystal Structures and Magnetic Properties of Novel [$Ln^{III}Cu^{II}_4$] (Ln = Gd, Dy, Ho) Pentanuclear Complexes. Topology and Ferromagnetic Interaction in the $Ln^{III}-Cu^{II}$ Pair

José Luis Sanz,[1a] Rafael Ruiz,[1a] Alain Gleizes,[1b] Francesc Lloret,*[,1a] Juan Faus,[1a] Miguel Julve,[1a] Juan José Borrás-Almenar,[1a] and Yves Journaux[1c]

Departament de Química Inorgànica, Facultat de Química de la Universitat de València, Dr. Moliner 50, 46100 Burjassot (València), Spain, Laboratoire des Matériaux, URA CNRS No. 445, INP Ecole Nationale Supérieure de Chimie de Toulouse, 118 Route de Narbonne, 31077 Toulouse, France, and Laboratoire de Chimie Inorganique, URA CNRS No. 420, Université de Paris-Sud, 91420 Orsay, France

Received May 10, 1996[⊗]

The first pentanuclear complexes of formula {Dy[Cu(apox)]$_2$[Cu(apox)(H_2O)]$_2$}[ClO_4]$_3$·7H_2O (**1**), {Ho[Cu(apox)]-[Cu(apox)(H_2O)]$_3$}[PF_6]$_3$·4.5H_2O (**2**), {Gd[Cu(apox)]$_2$[Cu(apox)(H_2O)]$_2$}[ClO_4]$_3$·7H_2O (**3**) and {Gd[Cu(apox)]-[Cu(apox) (H_2O)]$_3$}[PF_6]$_3$·4.5H_2O (**4**) (H_2apox = *N*,*N*′-bis(3-aminopropyl)oxamide) have been synthesized. The crystal structures of complexes **1** and **2** have been determined by X-ray diffraction methods. Complexes **3** and **4** are isostructural with **1** and **2**, respectively. Crystallographic data are as follows: **1** and **3**, monoclinic, space group *C*2/*c* and $Z = 4$, with $a = 14.646(6)$ Å, $b = 29.496(7)$ Å, $c = 16.002(7)$ Å, and $\beta = 111.76(2)°$ for **1** and $a = 14.523(6)$ Å, $b = 29.441(6)$ Å, $c = 15.925(8)$ Å, and $\beta = 111.90(4)°$ for **3**; **2** and **4**, triclinic, $P\bar{1}$, and $Z = 2$, with $a = 14.346(2)$ Å, $b = 14.454(2)$ Å, $c = 18.107(4)$ Å, $\alpha = 90.95(2)°$, $\beta = 110.75(2)°$, and $\gamma = 106.77(2)°$ for **2** and $a = 14.365(6)$ Å, $b = 14.496(5)$ Å, $c = 18.172(7)$ Å, $\alpha = 91.27(3)°$, $\beta = 110.74(3)°$, and $\gamma = 106.67-(3)°$ for **4**. A tripositive ion is present in these structures, the electroneutrality being achieved by three uncoordinated perchlorate (**1**) or hexafluorophosphate (**2**) anions. The lanthanide cations are eight-coordinate with a pseudo-square-antiprismatic environment formed by carbonyl oxygen atoms from two [Cu(apox)] and two Cu(apox)-(H_2O)] (**1**) and one [Cu(apox)] and three [Cu(apox)(H_2O)] (**2**) bidentate ligands. The temperature dependence of the magnetic susceptibility of complexes **1**−**4** was investigated in the range 1.8−300 K. The ligand-field effect, as well as the mixing of the free-ion states in Dy^{III} and Ho^{III}, make extremely difficult the analysis of the overall antiferromagnetic interaction which is observed for complexes **1** and **2**. The magnetic susceptibility data for complexes **3** and **4** have shown that the ground-state spin for the [$Gd^{III}Cu^{II}_4$] unit is $S = 11/2$, the $Gd^{III}-Cu^{II}$ interaction being ferromagnetic with an interaction parameter $J_{GdCu} = 0.85$ cm^{-1} (the interaction Hamiltonian is of the form $H = -JS_A \cdot S_B$). The field dependence of the magnetization at 2 K of **3** and **4** confirms the nature of the ground state and of the $Gd^{III}-Cu^{II}$ interaction. The influence of the topology and of the type of bridging ligand on the nature and magnitude of the magnetic interaction in the $Gd^{III}-Cu^{II}$ pair is analyzed and discussed in light of available magnetostructural data.

Introduction

The synthesis and characterization of oligonuclear complexes containing transition-metal and rare-earth ions have attracted the interest of magnetochemists since the pionnering work performed by Gatteschi and co-workers, who found that the $Gd^{III}-Cu^{II}$ interaction was ferromagnetic in a series of [Gd^{III}-Cu^{II}_2] trinuclear species,[2−4] where four phenolato oxygens from two bidentate Cu(II) Schiff base complexes act as bridges between both metal ions. The ferromagnetic nature of the magnetic interaction in the $Gd^{III}-Cu^{II}$ pair through a phenolate bridge (intramolecular Gd-Cu separation about 3.4 Å) not only for trimers but also for dimers has been confirmed by other authors.[5,6] The same synthetic strategy, which consists of using mononuclear copper(II) complexes as ligands with the appropriate gadolinium(III) salt, allowed the preparation of polynuclear complexes of formula [Gd(CuL)$_2$(H_2O)$_4$](NO_3)$_3$·H_2O (trinuclear),[7] {Gd[Cu(oxae)]$_3$}(ClO_4)$_3$ (tetranuclear),[8] Gd_2(ox)[Cu(pba)]$_3$-[Cu(H_2O)$_5$]·20H_2O (ladderlike structure),[9] and Gd_2{[Cu(pba)]}$_3$·23H_2O (tubelike structure)[10] (H_2L = *N*,*N*′-bis(3-amino-2,2-dimethylpropyl)oxamide, H_2oxae = *N*,*N*′-bis(2-aminoethyl)-oxamide, ox = oxalate dianion, and pba = 1,3-propylenebis-(oxamate) dianion). Again, the magnetic interaction between Gd^{III} and Cu^{II}, which are separated by more than 5.5 Å, is ferromagnetic, irrespective of the details of nuclearity and nature of the bridging ligand. To our knowledge, only in one case (the complex of formula GdCu(oxae)(phen)$_2$(ClO_4)$_3$,[11] where H_2oxae = *N*,*N*′-bis(2-aminoethyl)oxamide) is the interaction $Gd^{III}-Cu^{II}$ reported to be antiferromagnetic. A general orbital

⊗ Abstract published in *Advance ACS Abstracts,* November 1, 1996.

(1) (a) Universitat de València. (b) INP-Ecole Nationale Supérieure de Chimie de Toulouse. (c) Université de Paris-Sud.
(2) Bencini, A.; Benelli, C.; Caneschi, A.; Carlin, R. L.; Dei, A.; Gatteschi, D. *J. Am. Chem. Soc.* **1985**, *107*, 8128.
(3) Bencini, A.; Benelli, C.; Caneschi, A.; Dei, A.; Gatteschi, D. *Inorg. Chem.* **1986**, *25*, 572.
(4) Benelli, C.; Caneschi, A.; Gatteschi, D.; Guillou, O.; Pardi, L. *Inorg. Chem.* **1990**, *29*, 1750.
(5) (a) Matsumoto, N.; Sakamoto, M.; Tamaki, H.; Okawa, H.; Kida, S. *Chem. Lett.* **1990**, 853. (b) Sakamoto, M.; Hashimura, M.; Matsuki, K.; Matsumoto, N.; Inoue, K.; Okawa, H. *Bull. Chem. Soc. Jpn.* **1991**, *64*, 3639.
(6) Andruh, M.; Ramade, I.; Codjovi, E.; Guillou, O.; Kahn, O.; Trombe, J. C. *J. Am. Chem. Soc.* **1993**, *115*, 1822.
(7) Benelli, C.; Fabretti, A. C.; Giusti, A. *J. Chem. Soc., Dalton Trans.* **1993**, 409.
(8) Li, Y. T.; Jiang, Z. H.; Liao, D. Z.; Yan, S. P.; Ma, S. H.; Li, X. Y.; Wang, G. L. *Polyhedron* **1993**, *12*, 2781.
(9) Guillou, O.; Bergerat, P.; Kahn, O.; Bakalbassis, E.; Boubekeur, K.; Batail, P.; Guillot, M. *Inorg. Chem.* **1992**, *31*, 110.
(10) (a) Guillou, O.; Oushoorn, R. L.; Kahn, O.; Boubekeur, K.; Batail, P. *Angew. Chem., Int. Ed. Engl.* **1992**, *31*, 626. (b) Guillou, O.; Kahn, O.; Oushoorn, R. L.; Boubekeur, K.; Batail, P. *Inorg. Chim. Acta* **1992**, *198*−*200*, 119.
(11) Li, Y. T.; Jiang, Z. H.; Ma, S. L.; Li, X. Y.; Liao, D. Z.; Yan, S. P.; Wang, G. L. *Polyhedron* **1994**, *13*, 475.

S0020-1669(96)00524-1 CCC: $12.00

mechanism based on the ideas of Goodenough,[12] involving a charge transfer from the transition-metal ion (3d type orbitals) to the rare-earth cation (6s or 5d type orbitals),[4,6] has been invoked to account for the ferromagnetic nature of the $Gd^{III}-Cu^{II}$ interaction.

This paper is devoted essentially to the investigation of a new topology of compounds containing both Gd^{III} and Cu^{II} ions in order to check its influence on the ferromagnetic $Gd^{III}-Cu^{II}$ interaction. The replacement of gadolinium(III) by other lanthanide(III) ions with an angular momentum in the ground state is also explored. In the present work we describe the synthesis and magnetic characterization of novel $[Ln^{III}Cu^{II}_4]$ pentanuclear complexes of formula $\{Dy[Cu(apox)]_2[Cu(apox)(H_2O)]_2\}(ClO_4)_3\cdot 7H_2O$ (**1**), $\{Ho[Cu(apox)][Cu(apox)(H_2O)]_3\}(PF_6)_3\cdot 4.5H_2O$ (**2**), $\{Gd[Cu(apox)]_2[Cu(apox)(H_2O)]_2\}(ClO_4)_3\cdot 7H_2O$ (**3**), and $\{Gd[Cu(apox)][Cu(apox)(H_2O)]_3\}(PF_6)_3\cdot 4.5H_2O$ (**4**) (H_2apox = *N*,*N*′-bis(3-aminopropyl)oxamide) together with the crystal structures of **1** and **2**.

Experimental Section

Materials. The starting [Cu(apox)] complex and H_2apox were synthesized by the literature methods[13] from 3-aminopropane, diethyl oxalate, and copper hydroxide. $Ln(NO_3)_3\cdot 6H_2O$ (Ln = Gd, Dy, Ho) was prepared by reaction of an aqueous suspension of Ln_2O_3 with concentrated HNO_3 solutions followed by slow evaporation at room temperature. Potassium hexafluorophosphate and sodium perchlorate were purchased from commercial sources and used as received. Elemental analyses (C, H, N) were conducted by the Microanalytical Service of the Universidad Autónoma de Madrid. Copper contents were determined by absorption spectrometry.

Preparation of Complexes 1−4. All four complexes were prepared in a similar fashion and therefore, the synthesis of one of them, namely compound **2**, is detailed herein. Compound **2** was prepared as follows: an aqueous solution of $Ho(NO_3)_3\cdot 6H_2O$ (0.25 mmol, 5 mL) was added to an aqueous suspension of [Cu(apox)] (1 mmol, 20 mL). A clear violet solution was obtained with continuous stirring at room temperature after 1 h. Solid potassium hexafluorophosphate (1 mmol) was added to this solution, and purple parallelepipeds of **2**, which were suitable for X-ray analysis, separated from it by slow evaporation at room temperature after 24 h. They were filtered off and air-dried. Single crystals of **1** were obtained in a similar manner using perchlorate instead of hexafluorophosphate. They lose solvent easily and have to be kept in a freezer. Complexes **3** and **4** were obtained as polycrystalline powders by following procedures analogous to those used for **1** and **2**. **3** and **4** were found to be isostructural with **1** and **2**, respectively. Analytical data (C, H, N, Cu) for **1**−**4** agree well with their formula.

Instrumentation. IR spectra (KBr) pellets were taken on a Perkin-Elmer 1750 FTIR spectrometer. The diffuse-reflectance spectra of solid samples (Nujol mulls on filter paper) were measured with a Perkin-Elmer Lambda 9 UV/vis/near-IR recording spectrometer. Their magnetic susceptibilities were measured in the temperature range 1.8−300 K with a Metronique Ingenierie MS03 SQUID magnetometer, which was calibrated with $Hg[Co(NCS)_4]$. The magnetic susceptibilities in the high-temperature region were measured under an external field of 1 T, whereas a field of 200 G was used in the low-temperature region in order to avoid saturation effects. Moreover, given the great magnetic anisotropy that Dy(III) and Ho(III) cations can exhibit at low temperatures, the samples were fixed in the holder in order to avoid the reorientation of the crystallites in the field. Magnetization measurements at 2 K for complexes **3** and **4** were performed with the same SQUID magnetometer. Diamagnetic corrections were made with Pascal's constants[14] for all the constituent atoms.

Table 1. Crystallographic Data for $\{Dy[Cu(apox)]_2[Cu(apox)(H_2O)]_2\}(ClO_4)_3\cdot 7H_2O$ (**1**) and $\{Ho[Cu(apox)][Cu(apox)(H_2O)]_3\}(PF_6)_3\cdot 4.5H_2O$ (**2**)

	1	**2**
formula	$DyCu_4C_{32}H_{82}Cl_3N_{16}O_{29}$	$HoCu_4C_{32}H_{79}F_{18}N_{16}O_{15.5}P_3$
a, Å	14.646(6)	14.346(2)
b, Å	29.496(7)	14.454(2)
c, Å	16.002(7)	18.107(4)
α, deg	90	90.95(2)
β, deg	111.76(2)	110.75(2)
γ, deg	90	106.77(2)
V, Å^3	6420	3332
Z	4	2
fw	1678.12	1790.08
space group	*C*2/*c*	$P\bar{1}$
T, °C	20	20
ρ_{calcd}, g cm^{-3}	1.74	1.78
λ, Å	0.710 73	0.710 73
μ, cm^{-1}	25.5	25.0
R^a	0.048	0.048
$R_w{}^b$	0.069	0.069

^{a} $R = \sum(|F_o| - |F_c|)/\sum|F_o|$. ^{b} $R_w = [\sum w(|F_o| - |F_c|)^2/\sum wF_o^2]^{1/2}$.

X-ray Structure Determinations. Crystal systems, accurate cell constants, space groups, and intensity data for complexes **1** and **2** were obtained at room temperature from single crystals mounted on an Enraf-Nonius CAD4 diffractometer using graphite-monochromatized Mo Kα radiation (*λ* = 0.710 73 Å). Crystals of dimensions 0.15 × 0.25 × 0.67 mm^3 (**1**) and 0.10 × 0.16 × 0.67 mm^3 (**2**) were used. Since crystals of **1** decompose under ambient atmosphere, the selected crystal was sealed in a Lindeman glass capillary. This was not necessary for the crystal of **2**. Unit cell dimensions and crystal orientation matrices were obtained from least-squares refinement of 25 reflections. Crystal parameters and details of the refinement are summarized in Table 1. Compounds **3** and **4** are isostructural with **1** and **2**, respectively.[15] The intensities of three standard reflections measured every 2 h showed no significant variations. *ω*-scan (**1**) and *θ*−2*θ*-scan (**2**) modes were used to collect data up to maximum Bragg angles of 24° (**1**) and 23° (**2**). Intensities were corrected for Lorentz and polarization effects. They were not corrected for absorption, the crystals having a pseudo-cylinder shape due to small truncations and μR values less than 1. Of the 5193 (**1**) and 9520 (**2**) measured independent reflections, 3503 (**1**) and 6643 (**2**) were unique with $I > 3\sigma(I)$ and were used for the structure refinements.

Structure determinations were carried out by using Patterson and Fourier map techniques and refined by applying full-matrix least-squares techniques, using the program SHELX-76.[16] Throughout the refinement, the minimized function was $\sum w(|F_o| - |F_c|)^2$ with $w = 1/[\sigma^2(F_o) + qF_o^2]$ ($q = 0.0012(1)$ and $0.0015(2)$) and $|F_o|$ and $|F_c|$ being the observed and calculated structure factor amplitudes, respectively. The atomic scattering factors and anomalous terms are those of Cromer and Waber.[17] Some propyl carbon atoms were found to be disordered. Their site occupancies were refined as free variables and fixed in the last cycles of the refinement. Constraints were applied to C−C bonds of the disordered parts. Hydrogen atoms of $-NH_2$ and of nondisordered $-CH_2$ groups were introduced at calculated positions and treated using a riding model. Hydrogen atoms of both coordinated and noncoordinated water molecules could not be located. For both structures, some of the noncoordinated water molecules were found on sites too close to each other to be occupied simultaneously. They were given site occupancies of $^1/_2$. The molecule Ow(3) in **2** is spread over three

(12) Goodenough, J. B. *Magnetism and Chemical Bond*; Interscience: New York, 1963; p 165.
(13) (a) Journaux, Y.; Sletten, J.; Kahn, O. *Inorg. Chem.* **1985**, *24*, 4063. (b) Chang, H. J.; Volg, A. *J. Polym. Sci., Polym. Chem. Ed.* **1977**, *15*, 311.
(14) Selwood, P. W. *Magnetochemistry*; Interscience: New York, 1956; pp 78−91.
(15) Crystallographic data for **3** and **4** are as follows: **3**, monoclinic, space group *C*2/*c*, *a* = 14.523(6) Å, *b* = 29.441(6) Å, *c* = 15.925(8) Å, *β* = 111.90(4)°, *Z* = 4, and *V* = 6318 Å^3; **4**, triclinic, space group *P*1, *a* = 14.365(6) Å, *b* = 14.496(5) Å, *c* = 18.172(7) Å, α = 91.27(3)°, *β* = 110.74(3)°, *γ* = 106.67(3)°, *Z* = 2, and *V* = 3358 Å^3.
(16) (a) Sheldrick, G. M. SHELX-76, Program for Crystal Structure Determination; University of Cambridge, Cambridge, U.K., 1976. (b) Johnson, C. K. ORTEP, a Fortran Thermal Ellipsoid Program for Crystal Structure Illustrations; Report No. ORNL-3794; Oak Ridge National Laboratory, Oak Ridge, TN, 1965.
(17) Cromer, D. T.; Waber, J. T. *International Tables for X-ray Crystallography*; Kynoch Press: Birmingham, England, 1974.

positions with occupancies which were determined from the corresponding electron densities in the difference Fourier map. For some other noncoordinated water molecules full site occupancies led to excessively high isotropic displacement parameters. Their population parameters were estimated from the corresponding electron densities in the difference Fourier map. Two perchlorate anions of **1** were found disordered around 2-fold axes. Anisotropic displacement parameters were used, except for the oxygen atoms of one of the disordered perchlorates and all other disordered atoms. No significant feature appeared in the final difference-Fourier maps. The final cycle of refinement with 420 variables for **1** and 837 variables for **2** converged with the unweighted and weighted reliability factors which appear in Table 1. The largest parameter shift (in esd) was 0.19 for **1** and 0.21 for **2.** The maximum difference densities in the final map were 0.9 e $Å^{-3}$ for **1** and two peaks at 1.0 e $Å^{-3}$ close to the Ho atom for **2**. The values of the goodness of fit were 1.61 and 1.54 for **1** and **2**, respectively. The atomic positional parameters and equivalent isotropic thermal coefficients for non-hydrogen atoms are listed in Tables 2 (**1**) and 3 (**2**); selected bond lengths and angles are given in Tables 4 (**1**) and 5 (**2**). The Supporting Information contains crystal data, anisotropic thermal parameters, atomic parameters of hydrogen atoms, and complete lists of bond distances and angles (Tables S1−S7).

Results and Discussion

Description of the Structures. {Dy[Cu(apox)]$_2$[Cu(apox)(H$_2$O)]$_2$} [ClO$_4$]$_3$·7H$_2$O (1). The *C*-type, monoclinic unit cell of **1** comprises four cations of formula $\{Dy[Cu(apox)]_2[Cu(apox)(H_2O)]_2\}^{3+}$, three perchlorate anions, and seven noncoordinated water molecules. The cation (Figure 1) has the crystallographically imposed C_2 point symmetry. The labels a and b are used to distinguish atoms from [Cu(apox)] and [Cu(apox)(H$_2$O)], respectively. The copper coordination environment by four nitrogen atoms is essentially planar. In [Cu(apox)] the nitrogen atoms tetrahedrally deviate from their mean least-squares plane by ±0.18(3) Å on the average. In [Cu(apox)(H$_2$O)], the water coordination to copper is weak (Cu−O$_w$ = 2.41(2) Å) and completes the nitrogen planar environment to a square pyramid. The nitrogen atoms do not deviate significantly from their mean plane (±0.03(8) Å). The copper atom is only 0.10(8) Å above this plane. As expected, the amino nitrogens N(3) and N(4) have longer Cu-N bonds than the imino nitrogens N(1) and N(2). However, the difference is not as marked in [Cu(apox)(H$_2$O)] (Δ(Cu-N) = 0.028(8) Å on the average) as in [Cu(apox)] (0.052(7) Å). [Cu(apox)(H$_2$O)] also differs from [Cu(apox)] by the disorder of a carbon atom on one of the CuN_2C_3 cycles: C(4b) is distributed over two positions with unequal probabilities of 65% for C(41b) and 35% for C(42b). The bidentate coordination mode of both [Cu(apox)] and [Cu(apox)(H$_2$O)] fragments in **1** accounts for the significant lengthening of the oxamide carbonyl bonds (average C−O bond distance is 1.27 Å), as observed in other polynuclear compounds which contain chelating [Cu(apox)] ligands.[18] In the free [Cu(apox)] complex,[19] a shorter C−O bond (1.254(8) Å) is observed due to its greater double-bond character. Dysprosium is eight-coordinate with a pseudo-square-antiprismatic environment of oxygen atoms at distances ranging from 2.39 to 2.47 Å. The "square" bases are O(1a), O(2a), O(1b)^i, O(2b)^i and O(1a)^i, O(2a)^i, O(1b), O(2b), respectively, the superscript i indicating a position symmetrical through the 2-fold axis. They are roughly planar (maximum atom deviation from the mean plane is 0.13(2) Å) and quite parallel to the 2-fold axis (angle between normals is 1(2)°).

Table 2. Final Atomic Fractional Coordinates and Equivalent Isotropic Displacement Parameters[a,b] for Non-Hydrogen Atoms of Complex **1**

atom	*x*/*a*	*y*/*b*	*z*/*c*	U_{eq}, Å^2
Dy	0	0.07943(2)	1/4	0.0392(4)
Cu(a)	0.17183(7)	0.00599(3)	0.60081(7)	0.0348(6)
O(1a)	0.0008(4)	0.0146(2)	0.3424(4)	0.038(3)
O(2a)	0.0467(5)	0.0979(2)	0.4108(4)	0.043(3)
C(1a)	0.0600(6)	0.0174(3)	0.4230(6)	0.037(5)
C(2a)	0.0824(6)	0.0651(3)	0.4628(6)	0.035(5)
N(2a)	0.1390(5)	0.0661(2)	0.5478(5)	0.038(4)
C(3a)	0.1682(8)	0.1108(3)	0.5910(6)	0.055(6)
C(4a)	0.2367(8)	0.1060(3)	0.6871(6)	0.058(6)
C(5a)	0.1982(9)	0.0752(3)	0.7413(6)	0.061(6)
N(3a)	0.2150(6)	0.0282(2)	0.7278(5)	0.048(5)
N(1a)	0.1071(5)	−0.0141(2)	0.4770(4)	0.035(4)
C(6a)	0.1011(7)	−0.0595(3)	0.4397(6)	0.050(5)
C(7a)	0.1914(8)	−0.0869(3)	0.4950(7)	0.063(7)
C(8a)	0.2018(9)	−0.0947(3)	0.5892(7)	0.066(7)
N(4a)	0.2292(6)	−0.0545(2)	0.6466(5)	0.048(5)
Cu(b)	0.37959(8)	0.15178(4)	0.44426(8)	0.0459(7)
Ow(b)	0.458(1)	0.1484(4)	0.3359(9)	0.17(1)
O(1b)	0.1746(4)	0.0596(2)	0.3142(4)	0.038(3)
O(2b)	0.1042(4)	0.1433(2)	0.2614(4)	0.044(4)
C(1b)	0.2294(6)	0.0929(3)	0.3544(5)	0.036(5)
C(2b)	0.1914(6)	0.1402(3)	0.3212(6)	0.044(5)
N(2b)	0.2519(6)	0.1739(2)	0.3570(5)	0.050(5)
C(3b)	0.2158(9)	0.2202(3)	0.3286(9)	0.074(8)
C(41b)[c]	0.282(1)	0.2542(5)	0.394(1)	0.07(1)
C(42b)[d,e]	0.296(1)	0.253(1)	0.328(2)	0.09(1)
C(5b)	0.390(1)	0.2497(4)	0.410(1)	0.11(1)
N(3b)	0.4354(7)	0.2154(3)	0.4736(6)	0.069(6)
N(1b)	0.3152(5)	0.0913(2)	0.4178(5)	0.042(4)
C(6b)	0.3534(7)	0.0457(3)	0.4518(6)	0.055(6)
C(7b)	0.4324(7)	0.0483(4)	0.5450(6)	0.074(8)
C(8b)	0.5190(8)	0.0771(4)	0.548(1)	0.083(9)
N(4b)	0.4974(7)	0.1273(3)	0.5438(7)	0.078(7)
Cl(1)	1/2	0.0274(1)	1/4	0.063(2)
O(1p1)	0.4275(6)	−0.0007(3)	0.2619(6)	0.092(6)
O(2p1)	0.4535(7)	0.0542(3)	0.1726(6)	0.102(7)
Cl(2)	0	0.3156(2)	1/4	0.110(5)
O(1p2)	0	0.3608(7)	1/4	0.17(2)
O(2p2)[f]	0.089(2)	0.318(1)	0.334(2)	0.14(2)
O(3p2)[f]	0.008(3)	0.283(1)	0.199(3)	0.16(3)
O(4p2)[f]	0.062(3)	0.300(1)	0.201(3)	0.16(3)
Cl(3)[f]	0.4585(8)	0.3191(3)	0.2181(9)	0.14(1)
O(1p3)[d]	1/2	0.2768(5)	1/4	0.22(1)
O(2p3)[d,f]	0.495(3)	0.345(1)	0.297(2)	0.20(1)
O(3p3)[d,f]	0.447(3)	0.323(1)	0.127(1)	0.25(2)
O(4p3)[d,f]	0.362(1)	0.317(1)	0.214(2)	0.20(1)
Ow(1)	−0.0027(8)	0.1932(3)	0.4028(6)	0.101(7)
Ow(2)[f]	0.160(1)	0.2187(5)	0.055(1)	0.08(1)
Ow(3)[f]	0.359(1)	0.1997(5)	0.160(1)	0.09(1)
Ow(4)[d,g]	0.183(3)	0.309(1)	0.093(2)	0.22(2)
Ow(5)[d,h]	0.168(2)	0.311(1)	0.029(2)	0.15(1)
Ow(6)[d,f]	0.352(3)	0.278(2)	0.066(2)	0.20(2)

[a] Estimated standard deviations in the last significant digits are given in parentheses. [b] U_{eq} is defined as one-third of the trace of the orthogonalized $\mathbf{U}_{ij}$ tensor. [c] Population parameter 0.65. [d] Refined isotropically. [e] Population parameter 0.35. [f] Population parameter 0.50. [g] Population parameter 0.55. [h] Population parameter 0.45.

In both [Cu(apox)] and [Cu(apox)(H$_2$O)] units, the $DyO_2C_2N_2$-Cu fragments are folded around O(1a)···O(2a) (28.0(2)°) and O(1b)···O(2b) (26(3)°). Dysprosium-to-copper distances are 5.662(2) and 5.684(2) Å, respectively, and the distances between Cu(a) and Cu(b) are 6.299(2) and 6.980(2) Å.

Centrosymmetrically related Dy(apox)Cu fragments of adjacent cations partly overlap. The distance between centrosymmetrically related mean planes of oxamido groups is 3.28(3) Å. Dysprosium-to-copper and copper-to-copper distances between adjacent units are the shortest ones in the structure: 4.779(2) and 4.881(2) Å, respectively. There is no such overlap between [Cu(apox)(H$_2$O)] fragments.

(18) (a) Journaux, Y.; Sletten, J.; Kahn, O. *Inorg. Chem.* **1986**, *25*, 439. (b) Zhang, Z. Y.; Liao, Z. H.; Hao, S. Q.; Yao, X. K.; Wang, H. G.; Wang, G. L. *Inorg. Chim. Acta* **1990**, *173*, 201. (c) Mathonière, C.; Kahn, O.; Daran, J. C.; Hilbig, H.; Köhler, F. H. *Inorg. Chem.* **1993**, *32*, 4057.

(19) Sanz, J. L.; Cervera, B.; Ruiz, R.; Bois, C.; Faus, J.; Lloret, F.; Julve, M. *J. Chem. Soc., Dalton Trans.* **1996**, 1359.

Table 3. Final Atomic Fractional Coordinates and Equivalent Isotropic Displacement Parameters[a,b] for Non-Hydrogen Atoms of Complex **2**

atom	*x/a*	*y/b*	*z/c*	U_{eq}, Å^2	atom	*x/a*	*y/b*	*z/c*	U_{eq}, Å^2
Ho	0.26261(3)	0.00954(3)	0.24525(2)	0.0365(3)	C(1c)	0.2074(7)	−0.2175(6)	0.2422(5)	0.037(5)
Cu(a)	0.05157(8)	0.16496(8)	−0.02028(6)	0.0405(7)	C(2c)	0.1453(7)	−0.1914(7)	0.2879(5)	0.041(5)
Cu(b)	0.5365(1)	0.25975(8)	0.12184(7)	0.0534(8)	C(3c)	0.0515(9)	−0.2338(7)	0.3718(8)	0.084(9)
Cu(c)	0.1278(1)	−0.38317(8)	0.29865(8)	0.0557(8)	C(4c)	−0.032(1)	−0.3227(8)	0.377(1)	0.16(2)
Cu(d)	0.3114(1)	−0.01146(9)	0.56483(7)	0.0526(8)	C(5c)	0.000(2)	−0.412(1)	0.403(1)	0.19(2)
Ow(b)	0.6889(9)	0.3677(9)	0.2468(7)	0.126(9)	C(6c)	0.2684(9)	−0.3349(6)	0.1998(7)	0.072(7)
Ow(c)	0.276(1)	−0.399(1)	0.419(1)	0.18(1)	C(7c)	0.221(1)	−0.4409(7)	0.1627(9)	0.14(2)
Ow(d)	0.4914(6)	0.1190(5)	0.6569(4)	0.069(5)	C(8c)	0.210(1)	−0.5131(9)	0.221(1)	0.12(1)
O(1a)	0.1128(5)	0.0586(5)	0.1878(3)	0.049(4)	C(1d)	0.3426(7)	−0.0222(6)	0.4233(5)	0.037(5)
O(2a)	0.2071(5)	−0.0032(4)	0.1045(3)	0.051(4)	C(2d)	0.2928(7)	0.0580(7)	0.4221(5)	0.042(6)
O(1b)	0.3324(5)	0.1728(4)	0.2289(4)	0.053(4)	C(3d)	0.223(1)	0.149(1)	0.4838(7)	0.11(1)
O(2b)	0.4228(5)	0.0382(4)	0.2272(4)	0.045(4)	C(4d1)[c,e]	0.231(2)	0.183(1)	0.5662(8)	0.075(6)
O(1c)	0.2470(5)	−0.1509(4)	0.2064(4)	0.051(4)	C(4d2)[c,f]	0.145(1)	0.119(3)	0.525(1)	0.11(1)
O(2c)	0.1360(5)	−0.1055(4)	0.2838(4)	0.047(4)	C(5d)	0.190(1)	0.104(1)	0.611(1)	0.17(2)
O(1d)	0.3632(5)	−0.0400(4)	0.3639(3)	0.046(4)	C(6d)	0.398(1)	−0.1484(8)	0.4883(6)	0.078(8)
O(2d)	0.2716(5)	0.0963(4)	0.3582(3)	0.050(4)	C(7d1)[c,g]	0.436(1)	−0.177(1)	0.5716(6)	0.074(4)
N(1a)	0.0527(6)	0.1485(5)	0.0873(4)	0.048(5)	C(7d2)[c,h]	0.341(4)	−0.228(2)	0.525(2)	0.11(2)
N(2a)	0.1477(6)	0.0865(6)	0.0059(4)	0.047(5)	C(8d)	0.356(1)	−0.199(1)	0.6104(8)	0.11(1)
N(3a)	0.0593(6)	0.1793(6)	−0.1279(5)	0.053(5)	P(1)	0.0599(3)	0.7476(3)	0.6484(2)	0.080(2)
N(4a)	−0.0560(6)	0.2335(6)	−0.0452(5)	0.054(5)	P(2)	0.1483(2)	0.4743(2)	−0.0917(2)	0.068(2)
N(1b)	0.4267(6)	0.2637(6)	0.1606(5)	0.058(5)	P(3)	0.5517(3)	0.7537(2)	0.1544(2)	0.074(2)
N(2b)	0.5140(6)	0.1302(5)	0.1577(5)	0.047(5)	F(11)	0.046(1)	0.6865(7)	0.7156(6)	0.150(9)
N(3b)	0.6458(8)	0.2488(7)	0.0810(6)	0.086(7)	F(21)	0.147(1)	0.830(1)	0.7048(7)	0.18(1)
N(4b)	0.5372(9)	0.3836(7)	0.0718(6)	0.098(8)	F(31)	0.074(1)	0.8087(8)	0.5802(7)	0.17(1)
N(1c)	0.2106(6)	−0.3055(5)	0.2423(5)	0.049(5)	F(41)	−0.027(1)	0.662(1)	0.5870(7)	0.17(1)
N(2c)	0.1092(6)	−0.2586(6)	0.3242(5)	0.054(5)	F(51)	−0.017(2)	0.791(1)	0.657(1)	0.31(2)
N(3c)	0.030(1)	−0.4611(8)	0.3476(9)	0.14(1)	F(61)	0.129(2)	0.698(2)	0.635(1)	0.38(3)
N(4c)	0.1315(9)	−0.5123(6)	0.2536(7)	0.091(8)	F(12)	0.2382(8)	0.5579(6)	0.9696(6)	0.121(7)
N(1d)	0.3569(6)	−0.0644(6)	0.4874(5)	0.053(5)	F(22)	0.1608(7)	0.3992(6)	0.9697(5)	0.105(6)
N(2d)	0.2754(7)	0.0752(6)	0.4846(5)	0.061(6)	F(32)	0.0558(8)	0.3914(6)	0.8456(6)	0.121(7)
N(3d)	0.2405(8)	0.0320(8)	0.6320(6)	0.078(7)	F(42)	0.1341(8)	0.5483(6)	0.8467(6)	0.130(7)
N(4d)	0.3491(8)	−0.1070(7)	0.6388(5)	0.070(6)	F(52)	0.070(1)	0.497(1)	0.9407(9)	0.21(1)
C(1a)	0.1010(7)	0.0874(7)	0.1191(5)	0.041(5)	F(62)	0.225(1)	0.448(1)	0.8793(8)	0.22(1)
C(2a)	0.1565(7)	0.0527(6)	0.0732(5)	0.035(5)	F(13)	0.490(1)	0.8156(9)	0.170(1)	0.30(2)
C(3a)	0.2083(8)	0.0648(8)	−0.0369(5)	0.065(7)	F(23)	0.5637(9)	0.8084(9)	0.0834(6)	0.16(1)
C(4a)	0.1651(8)	0.0721(6)	−0.1252(5)	0.060(7)	F(33)	0.609(1)	0.6913(9)	0.137(1)	0.25(2)
C(5a)	0.1516(8)	0.1713(6)	−0.1406(6)	0.06(7)	F(43)	0.535(1)	0.700(1)	0.2234(8)	0.19(1)
C(6a)	0.0080(9)	0.1941(7)	0.1335(6)	0.071(7)	F(53)	0.6543(9)	0.831(1)	0.2058(7)	0.18(1)
C(7a)	−0.028(1)	0.2760(9)	0.0943(6)	0.13(1)	F(63)	0.4480(8)	0.6750(8)	0.1001(6)	0.138(8)
C(8a)	−0.107(1)	0.246(1)	0.0094(6)	0.12(1)	Ow(1)	0.512(1)	0.3056(9)	0.5876(9)	0.16(1)
C(1b)	0.3980(7)	0.1897(6)	0.1953(6)	0.043(6)	Ow(2)	0.003(1)	−0.009(1)	0.3242(9)	0.17(1)
C(2b)	0.4497(7)	0.1132(6)	0.1932(5)	0.039(5)	Ow(3a)[i]	0.251(1)	0.281(1)	0.3095(8)	0.085(4)
C(3b)	0.5576(9)	0.0537(8)	0.1501(6)	0.067(7)	Ow(3b)[j]	0.426(4)	0.389(4)	0.436(3)	0.10(1)
C(4b)	0.610(1)	0.072(1)	0.091(1)	0.16(2)	Ow(3c)[j]	0.356(3)	0.301(30	0.364(3)	0.09(1)
C(5b)	0.689(1)	0.1705(9)	0.099(1)	0.21(2)	Ow(4)[c,d]	0.240(3)	0.399(2)	0.407(2)	0.19(1)
C(6b)	0.374(1)	0.3381(7)	0.1585(8)	0.087(9)	Ow(5)[c,d]	0.320(3)	0.463(3)	0.690(2)	0.23(2)
C(7b)	0.411(2)	0.427(1)	0.121(1)	0.21(2)	Ow(6)[c,k]	0.327(4)	0.867(3)	0.070(3)	0.12(1)
C(8b1)[c,d]	0.505(2)	0.460(1)	0.096(2)	0.083(7)	Ow(7)[c,d]	0.367(4)	0.568(4)	0.636(3)	0.13(2)
C(8b2)[c,d]	0.444(2)	0.414(2)	0.051(1)	0.091(8)					

[a] Estimated standard deviations in the last significant digits are given in parentheses. [b] U_{eq} is defined as one-third of the trace of the orthogonalized $\mathbf{U}_{ij}$ tensor. [c] Refined isotropically. [d] Population parameter 0.50. [e] Population parameter 0.56. [f] Population parameter 0.44. [g] Population parameter 0.77. [h] Population parameter 0.23. [i] Population parameter 0.60. [j] Population parameter 0.20. [k] Population parameter 0.25.

{Ho[Cu(apox)][Cu(apox)(H$_2$O)]$_3$}[PF$_6$]$_3$·4.5H$_2$O (2). The triclinic unit cell comprises two cations of formula $\{Ho[Cu(apox)][Cu(apox)(H_2O)]_3\}^{3+}$, two hexafluorophosphate anions, and four and a half noncoordinated water molecules. Label a denotes the [Cu(apox)] fragment, and labels b−d indicate the [Cu(apox)(H$_2$O)] units. A view of the cation is given in Figure 2. The nitrogen 4-fold environment of copper atoms does not depart significantly from planarity: atom-to-mean-plane distances are ±0.05(8) Å for a, ±0.06(6) Å for b, ±0.03(8) Å for c, and ±0.07(15) Å for d. For ligands b−d, water-to-copper coordinations are weak (2.60(1), 2.51(1), and 2.65(1) Å for Cu(b)−Ow(b), Cu(c)−Ow(c), and Cu(d)−Ow(d), respectively) and complete copper environments to square pyramids in which the cations are about 0.1 Å above bases. Disorder occurs with split positions for carbons C(8b), C(4d), and C(7d). Holmium has a pseudo-square-antiprismatic environment of oxygen atoms at distances ranging from 2.34 to 2.40 Å.

The "square" bases, made up of atoms O(1a), O(2a), O(1c), O(2c) and O(1b), O(2b), O(1d), O(2d) are quite planar (maximum atom-to-mean-plane deviations 0.07(17) and 0.012(3) Å, respectively) and parallel (angle between normals 1(4)°). Folding angles of 26.9(5), 21.7(2), 20(3), and 23(4)° are observed around segments O(1)···O(2) for ligands a−d, respectively. Holmium-to-copper distances are 5.594(1), 5.639(1), 5.663(1), and 5.601(1) Å, respectively.

Centrosymmetrically related Ho(apox)Cu fragments of adjacent cations partially overlap. The distance between centrosymmetrically related mean planes of oxamido groups is 3.57(4) Å. Holmium-to-copper and copper-to-copper distances between ajacent units are the shortest ones in the structure: 4.833(1) and 4.720(2) Å, respectively. As in **1**, hydrated Cu(apox)(H$_2$O) fragments do not overlap.

IR and Electronic Spectra. Apart from the absorption features attributed to the uncoordinated perchlorate and hexa-

Table 4. Selected Bond Lengths (Å) and Angles (deg) for Complex **1**[a]

Around Dy (Point Symmetry 2)			
Dy−O(1a)	2.416(6)	Dy−O(1b)	2.448(5)
Dy−O(2a)	2.466(6)	Dy−O(2b)	2.389(6)
O(1a)−Dy−O(2a)	66.42(19)	O(2a)−Dy−O(2b)	79.83(21)
O(1a)−Dy−O(1b)	77.64(20)	O(2a)−Dy−O(2a)^{i}	154.42(26)
O(1a)−Dy−O(2b)	136.06(17)	O(2a)−Dy−O(1b)^{i}	109.50(22)
O(1a)−Dy−O(1a)^{i}	75.26(29)	O(2a)−Dy−O(2b)^{i}	80.06(20)
O(1a)−Dy−O(2a)^{i}	138.65(18)	O(1b)−Dy−O(2b)	67.58(18)
O(1a)−Dy−O(1b)^{i}	80.50(19)	O(1b)−Dy−O(1b)^{i}	152.30(25)
O(1a)−Dy−O(2b)^{i}	121.99(23)	O(2b)−Dy−O(2b)^{i}	139.38(18)
O(2a)−Dy−O(1b)	76.83(21)	O(2b)−Dy−O(2b)^{i}	75.81(29)
Around Cu			
Cu(a)		Cu(b)	
Cu(a)−N(1a)	1.945(6)	Cu(b)−N(1b)	1.989(7)
Cu(a)−N(2a)	1.946(7)	Cu(b)−N(2b)	1.985(7)
Cu(a)−N(3a)	2.001(7)	Cu(b)−N(3b)	2.031(9)
Cu(a)−N(4a)	1.993(7)	Cu(b)−N(4b)	2.000(9)
		Cu(b)−Ow(b)	2.414(17)
N(1a)−Cu(a)−N(2a)	83.39(27)	N(1b)−Cu(b)−N(2b)	84.05(28)
N(1a)−Cu(a)−N(3a)	170.1(3)	N(1b)−Cu(b)−N(3b)	175.1(4)
N(1a)−Cu(a)−N(4a)	94.68(28)	N(1b)−Cu(b)−N(4b)	92.6(3)
N(2a)−Cu(a)−N(3a)	94.56(29)	N(2b)−Cu(b)−N(3b)	93.0(3)
N(2a)−Cu(a)−N(4a)	167.9(4)	N(2b)−Cu(b)−N(4b)	171.6(4)
N(3a)−Cu(a)−N(4a)	89.29(29)	N(3b)−Cu(b)−N(4b)	89.7(4)
		Ow(b)−Cu(b)−N(1b)	97.2(4)
		Ow(b)−Cu(b)−N(2b)	94.8(4)
		Ow(b)−Cu(b)−N(3b)	86.9(4)
		Ow(b)−Cu(b)−N(4b)	93.2(5)
Closest Distances between Cations			
Dy···Cu(a)^{ii}	4.7786(16)	Cu(a)···Cu(a)^{ii}	4.8813(24)
Dy···Cu(a)	5.6625(23)	Cu(a)···Cu(b)	6.2991(21)
Dy···Cu(b)	5.6843(21)	Cu(a)···Cu(b)^{iii}	6.9800(23)

[a] Symmetry operations: (i) $-x$, y, $^1/_2 - z$; (ii) $-x$, $-y$, $-z$; (iii) x, $-y$, $^1/_2 + z$.

Table 5. Selected Bond Lengths (Å) and Angles (deg) for Complex **2**[a]

Around Ho			
Ho−O(1a)	2.350(7)	Ho−O(1c)	2.335(7)
Ho−O(2a)	2.372(6)	Ho−O(2c)	2.397(6)
Ho−O(1b)	2.351(6)	Ho−O(1d)	2.379(6)
Ho−O(2b)	2.356(7)	Ho−O(2d)	2.325(7)
O(1a)−Ho−O(2a)	68.15(25)	O(1b)−Ho−O(1c)	143.66(28)
O(1a)−Ho−O(1b)	76.67(23)	O(1b)−Ho−O(2c)	146.59(27)
O(1a)−Ho−O(2b)	134.93(23)	O(1b)−Ho−O(1d)	114.89(19)
O(1a)−Ho−O(1c)	116.74(20)	O(1b)−Ho−O(2d)	76.80(24)
O(1a)−Ho−O(2c)	78.05(22)	O(2b)−Ho−O(1c)	81.05(23)
O(1a)−Ho−O(1d)	142.75(26)	O(2b)−Ho−O(2c)	143.97(23)
O(1a)−Ho−O(2d)	81.19(23)	O(2b)−Ho−O(1d)	79.56(23)
O(2a)−Ho−O(1b)	79.29(21)	O(2b)−Ho−O(2d)	115.48(21)
O(2a)−Ho−O(2b)	78.19(23)	O(1c)−Ho−O(2c)	68.43(26)
O(2a)−Ho−O(1c)	75.86(22)	O(1c)−Ho−O(2c)	68.43(26)
O(2a)−Ho−O(2c)	110.77(20)	O(1c)−Ho−O(2d)	136.21(23)
O(2a)−Ho−O(1d)	146.33(26)	O(2c)−Ho−O(1d)	74.95(21)
O(2a)−Ho−O(2d)	144.65(24)	O(2c)−Ho−O(2d)	78.06(22)
O(1b)−Ho−O(2b)	68.12(25)	O(1d)−Ho−O(2d)	68.53(24)
Around Cu(j)				
	j = a	j = b	j = c	j = d
Cu(j)−N(1j)	1.961(8)	1.951(11)	1.959(9)	1.968(10)
Cu(j)−N(2j)	1.967(7)	1.968(8)	1.966(9)	1.962(9)
Cu(j)−N(3j)	2.001(9)	1.998(13)	2.004(16)	2.032(13)
Cu(j)−N(4j)	1.993(9)	2.019(10)	2.046(11)	1.993(10)
Cu(j)−Ow(j)		2.597(9)	2.507(15)	2.653(6)
N(1j)−Cu(j)−N(2j)	84.1(4)	82.9(4)	83.5(4)	82.9(4)
N(1j)−Cu(j)−N(3j)	176.1(4)	177.2(3)	174.2(3)	170.7(3)
N(1j)−Cu(j)−N(4j)	93.2(4)	93.9(5)	93.3(5)	92.1(4)
N(1j)−Cu(j)−Ow(j)		94.5(4)	98.7(5)	100.1(3)
N(2j)−Cu(j)−N(3j)	92.3(4)	94.7(4)	94.5(5)	94.4(5)
N(2j)−Cu(j)−N(4j)	171.1(3)	174.5(3)	170.7(4)	174.8(4)
N(2j)−Cu(j)−Ow(j)		101.5(3)	105.1(4)	94.4(3)
N(3j)−Cu(j)−N(4j)	90.5(4)	88.3(5)	87.8(5)	90.4(5)
N(3j)−Cu(j)−Ow(j)		87.3(4)	87.1(6)	88.9(3)
N(4j)−Cu(j)−N(2j)		86.9(4)	84.0(5)	87.75(28)
Closest Distances between Cations				
Ho···Cu(1)^{i}	4.8333(10)	Cu(1)···Cu(1)^{i}	4.7205(24)	
Ho···Cu(1)	5.5943(12)	Cu(1)···Cu(2)	6.2124(20)	
Ho···Cu(2)	5.6390(15)	Cu(1)···Cu(3)^{i}	6.1638(17)	
Ho···Cu(3)	5.6627(15)	Cu(2)···Cu(4)^{ii}	6.8005(19)	
Ho···Cu(4)	5.6014(14)	Cu(3)···Cu(4)	6.4042(19)	
Ho···Cu(4)^{ii}	5.8462(16)	Cu(4)···Cu(4)^{ii}	6.549(3)	

[a] Symmetry operations: (i) $-x$, $-y$, $-z$; (ii) $1 - x$, $-y$, $1 - z$.

fluorophosphate groups, compounds **1**−**4** display practically identical IR spectra. The most relevant feature is the occurrence of the ν(N−C−O) stretching bands at 1605 (s) (it appears at 1586 (s) cm^{-1} in the free [Cu(apox)]) and 1445 (m) cm^{-1}, which are characteristic of the bridging oxamido group.[20] Moreover, the δ(CO) deformation peak, which is centered at 710 (m) cm^{-1} in the uncoordinated [Cu(apox)], is lacking in the spectra of the pentanuclear complexes. This fact may be attributed to the coordination of the carbonyl oxygen atoms to either transition-metal ions[21] or lanthanide cations.[8]

The reflectance spectra of complexes **1** and **2** show sharp peaks corresponding to the f−f transitions of the lanthanide cations which are obscured by a broad peak centered at 18 520 cm^{-1} (complexes **1**−**4**) that is tentatively assigned to the d-d transition in coordinated [Cu(apox)]. The fact that this band is shifted to 20 400 cm^{-1} in free [Cu(apox)] is consistent with the expected weakening of the ligand field in the [CuN_4] chromophore because of the coordination of [Cu(apox)] in **1**−**4**.

Magnetic Properties. Complexes 3 and 4. The thermal dependences of $\chi_M T$ (χ_M being the magnetic susceptiblity for the [$Ln^{III}Cu^{II}_4$] pentanuclear unit) for compounds **3** and **4** are practically identical. For the sake of brevity, only the magnetic properties of **3** are shown in Figure 3. $\chi_M T$ is equal to 9.40 cm^3 mol^{-1} K at room temperature, a value which is as expected for a Gd(III) ion and four Cu(II) ions that do not interact. When the temperature is lowered, $\chi_M T$ first remains constant up to 50 K and increases regularly at lower temperatures, reaching a value of 16.4 cm^3 mol^{-1} K at 1.8 K. This behavior is typical of a Gd(III)−Cu(II) ferromagnetic interaction. Keeping in mind the structure of complex **3** (isostructural with **1**), its magnetic properties have been interpreted with a Hamiltonian of the form

$$\hat{H} = -J_{GdCu}\hat{S}_{Gd}\cdot(\hat{S}_{Cu1} + \hat{S}_{Cu2} + \hat{S}_{Cu3} + \hat{S}_{Cu4}) - J_{CuCu}[\hat{S}_{Cu1}\cdot(\hat{S}_{Cu2} + \hat{S}_{Cu3} + \hat{S}_{Cu4}) + \hat{S}_{Cu2}\cdot(\hat{S}_{Cu3} + \hat{S}_{Cu4}) + \hat{S}_{Cu3}\cdot\hat{S}_{Cu4}) \quad (1)$$

where J_{GdCu} and J_{CuCu} account for the Gd(III)−Cu(II) and peripheral Cu(II)−Cu(II) magnetic interactions, respectively. Least-squares minimization of the susceptibility data of complex **3** through the corresponding expression for the susceptibility derived from the Hamiltonian (1)[22a] leads to $J_{GdCu} = 0.85$ cm^{-1}, $J_{CuCu} = -0.40$ cm^{-1}, $g_{Gd} = 2.0$, $g_{Cu} = 2.08$, and $R = 1.4 \times 10^{-4}$. R is the agreement factor, defined as $\sum[(\chi_M T)^{obsd} - (\chi_M T)^{calcd}]^2/\sum[(\chi_M T)^{obsd}]^2$. The corresponding values for complex **4** are $J_{GdCu} = 0.80$ cm^{-1}, $J_{CuCu} = -0.65$ cm^{-1}, $g_{Gd} = 2.0$,

(20) (a) Ojima, H.; Nonoyama, K. *Z. Anorg. Allg. Chem.* **1972**, *389*, 75. (b) Radecka-Paryzeck, W. *Inorg. Chim. Acta* **1979**, *34*, 5. (c) Ojima, H.; Nonoyama, K. *Coord. Chem. Rev.* **1988**, *92*, 85.

(21) (a) Okawa, H.; Kawahara, Y.; Mykuriya, M.; Kyda, S. *Bull. Chem. Soc. Jpn.* **1980**, *53*, 549. (b) Lloret, F.; Journaux, Y.; Julve, M. *Inorg. Chem.* **1990**, *29*, 3967.

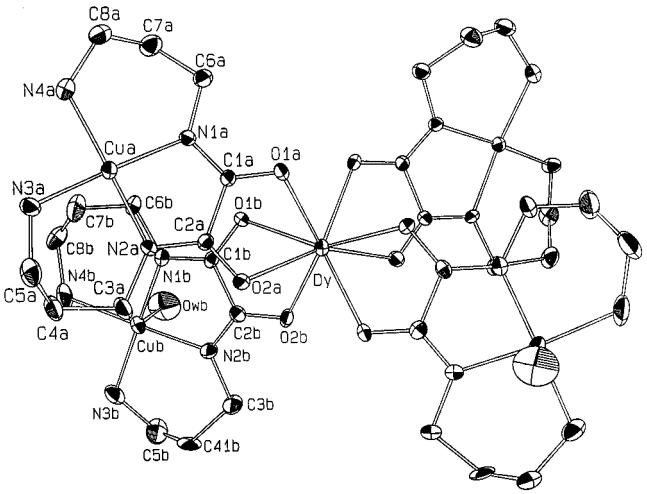

Figure 1. View of the heteropentanuclear cation $\{Dy[Cu(apox)]_2[Cu(apox)(H_2O)]_2\}^{3+}$ (**1**) with the atom-labeling scheme. Hydrogen atoms have been omitted for clarity. The thermal ellipsoids are drawn at the 30% probability level.

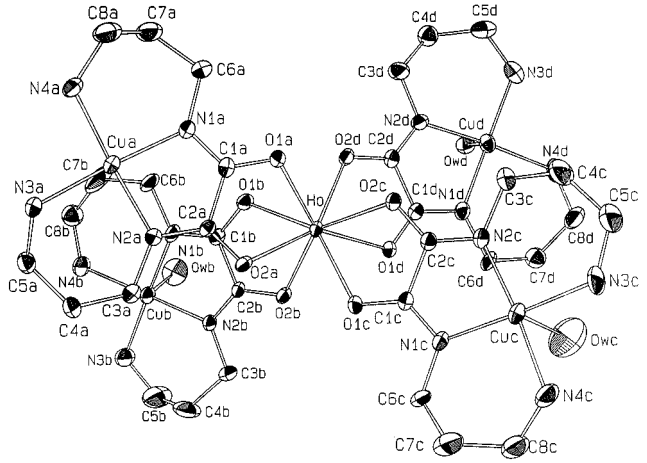

Figure 2. View of the heteropentanuclear cation $\{Ho[Cu(apox)][Cu(apox)(H_2O)]_3\}^{3+}$ (**2**) showing the atom-labeling scheme. Hydrogen atoms have been omitted for clarity.

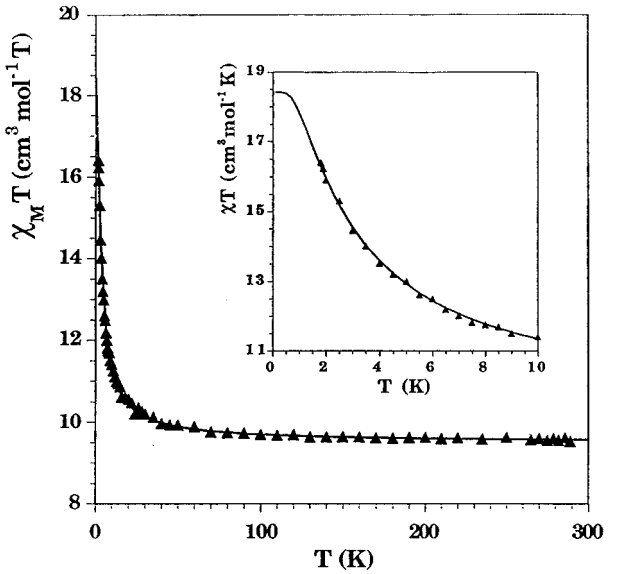

Figure 3. $\chi_M T$ versus T plot for complex **3**. The inset shows the lower temperature region.

$g_{Cu} = 2.07$, and $R = 1.6 \times 10^{-4}$. In order to confirm the nature of the ground state, $S = 11/2$, we investigated the variation of the magnetization M versus the field H at 2 K. The magnetization curve of **3** (Figure 4) closely follows the Brillouin function for a spin $S = 11/2$ with $g_{11/2,2} = 2.03$, and it is very different from the curve for five independent local spins (that is, one $S_{Gd} = 7/2$ and four $S_{Cu} = 1/2$), indicating that the ground state $S = 11/2$ is nearly populated at 2 K. These data unambiguously show that the magnetic interaction between the peripheral copper(II) ions and the central gadolinium(III) cation is ferromagnetic and dominates the antiferromagnetic interaction between the peripheral Cu(II) ions. Both the ferromagnetic $Gd^{III}-Cu^{II}$ coupling and the antiferromagnetic interaction between Cu(II) ions through Gd(III) are commonly observed in the polynuclear $Gd^{III}-Cu^{II}$ complexes. The values of J_{CuCu} in **3** and **4** (-0.40 and -0.65 cm^{-1}) are of the same order although somewhat smaller than those observed in the tetranuclear $\{Cd[Cu(apox)]_3\}(NO_3)_2 \cdot 2H_2O$ ($J_{CuCu} = -1.45$ cm^{-1})[21b] and trinuclear $\{Zn[Cu(apox)]_2\}(ClO_4)_2 \cdot 2H_2O$ ($J_{CuCu} = -1.6$ cm^{-1})[18a] apox-bridged metal complexes.

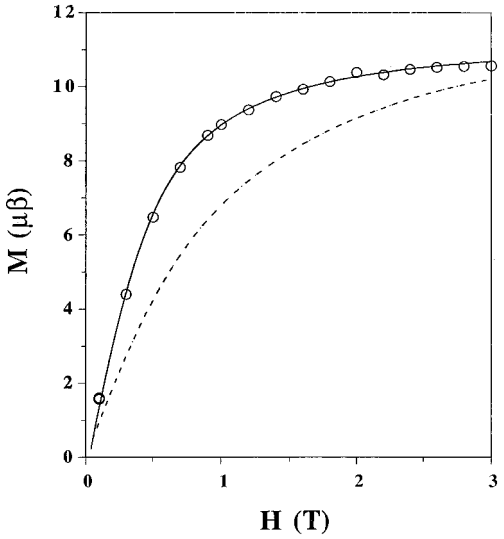

Figure 4. Field dependence of the magnetization for complex **3** at 2 K: (○) experimental data; (−) Brillouin function for a spin $S = 11/2$ with $g = 2.03$; (- - -) Brillouin function for a local spin $S_{Gd} = 7/2$ and four local spins $S_{Cu} = 1/2$.

Different spin ground states can result in $[Gd^{III}Cu^{II}_4]$ because of the competition between the weak ferromagnetic J_{GdCu} and next-nearest-neighbor antiferromagnetic J_{CuCu} interactions. Thus in Figure 5, for instance, we have considered the different energy levels which would be obtained as a function of the J_{CuCu}/J_{GdCu} (α) ratio, considering that the Gd(III)−Cu(II) and Cu(II)−Cu(II) magnetic interactions are ferro- and antiferromagnetic, respectively (Figure 5a). The shape of the corresponding $\chi_M T$ curves is shown in Figure 5b. As shown in Figure 5a, the ground state may be $S = 11/2$ ($|\alpha| < 1.75$), $S = 9/2$ ($1.75 < |\alpha| < 3.5$), and $S = 7/2$ ($|\alpha| > 3.5$ or may even be degenerate ($|\alpha|$ ca. 1.75 or 3.5; cases of spin frustration).[23] Therefore, the shapes of the $\chi_M T$ curves can be dramatically different, as shown in Figure 5b, since overall ferromagnetic ($|\alpha| < 3$) to overall antiferromagnetic ($|\alpha| > 4$) behavior passes through a nearly Curie law ($3 < |\alpha| < 4$) situation. Curiously, this kind of compound can exhibit a maximum of $\chi_M T$ ($|\alpha|$ ca. 2 in Figure 5b), which is due to an irregular spin state structure where states

(22) (a) The energies $E(S,S')$ of the low-lying states deduced from the Hamiltonian (1) and and the theoretical expression for the magnetic susceptibility are given in Appendix A in the Supporting Information. (b) The calculational methods to evaluate this set of parameters are detailed in Appendix B in the Supporting Information.

(23) Hendrickson, D. N. In *Research Frontiers in Magnetochemistry*; O'Connor, C. J., Ed.; World Scientific: Singapore, 1993; p 87, and references therein.

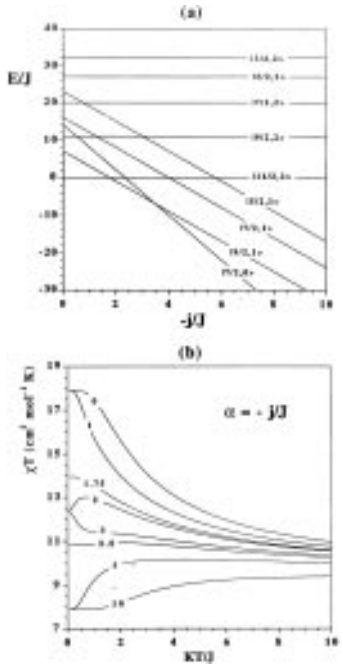

Figure 5. (a) Energy levels of a pentanuclear $[Gd^{III}Cu^{II}_4]$ unit for J_{GdCu} (**J**) > 0 and J_{CuCu} (**j**) < 0. Each state is labeled as $|S,S'>$, and its energy is given in units of the exchange parameter J_{GdCu}. (b) Shapes of the $\chi_M T$ curves as a function of $-\alpha$ for the case (a).

of maximum spin multiplicity are intermediate in energy. This situation is opposite that observed in the well-known examples of irregular spin state structure dealing with heteropolynuclear compounds with first-row transition-metal ions, where the states of minimum multiplicity are intermediate in energy.[24] Finally, it is important to note that the occurrence of nearly Curie law behavior in this kind of compound is in principle not a sign of a lack of magnetic interaction and would correspond to $|\alpha|$ values close to 3.5. These observations reveal that a detailed analysis of both Gd(III)−Cu(II) and Cu(II)−Cu(II) magnetic interactions is of utmost importance in order to analyze properly the susceptibility data of such systems, because as shown in Figure 5, the overall antiferromagnetic behavior is not neccessarily due to a Gd(III)−Cu(II) antiferromagnetic interaction. In fact, when the Gd(III)−Cu(II) magnetic interaction is antiferromagnetic, the $\chi_M T$ curves are very different, as shown in Figure 6, where both J_{GdCu} and J_{CuCu} are assumed to be antiferromagnetic. A more pronounced overall antiferromagnetic behavior is observed for this case. It is important to note that, for $|\alpha| > 4.5$, a minimum of $\chi_M T$ can be observed as expected for a classical irregular spin structure situation (Figure 6a for $|\alpha| > 4.5$).

Although in general the experimental range of the values for α is not as large (from -0.47 to -3 cm^{-1})[2-7] as that used in Figures 5 and 6, it can be very large for the Gd^{III}−radical systems, where values of $J_{rad-rad}/J_{Gd-rad}$ up to -13 cm^{-1} have been achieved.[25-27] It should be noted that this phenomenon arises from the fact that the interaction between the nearest-neighbor cations (Gd^{III}−Cu^{II}) can be weaker than that between next-nearest-neighbor ions (Cu^{II}−Cu^{II}). This contrasts with what is observed for most of the polynuclear systems involving only transition-metal ions or radical and transition-metal ions,

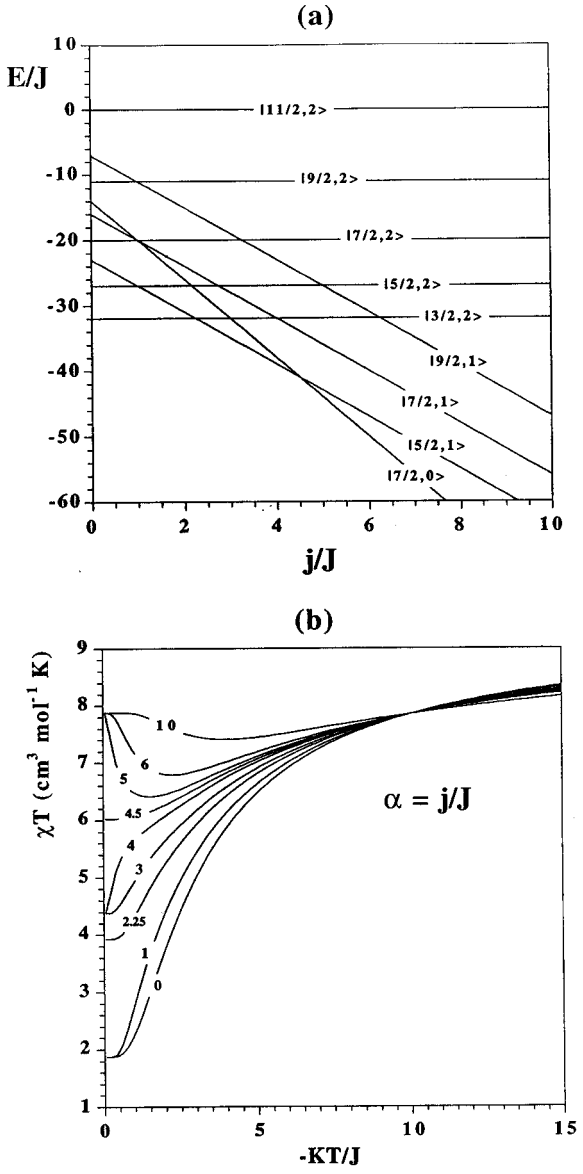

Figure 6. (a) Energy levels of a pentanuclear $[Gd^{III}Cu^{II}_4]$ unit for J_{GdCu} (**J**) < 0 and J_{CuCu} (**j**) < 0. (b) Shapes of the $\chi_M T$ curves as a function of α for the case (a).

where the former interaction is much larger than the latter and, consequently, the competition between them does not occur. This can led to exotic magnetic curves that are rarely observed in other systems. In order to understand this ferromagnetic interaction, a model has already been suggested which involves the transfer of electron density from the Cu(II) ion into an empty orbital of the rare-earth ion.[28] This fraction of unpaired electron polarizes the unpaired electrons of the inner f orbitals, thus giving rise to parallel alignment of the spins. Obviously, if this is the mechanism which leads to the ferromagnetic coupling, it should work in other copper−lanthanide systems. This is why we undertook the magnetic study of the $DyCu_4$ (**1**) and $HoCu_4$ (**2**) complexes.

Complexes 1 and 2. The magnetic behaviors of compounds **1** and **2** in the form of $\chi_M T$ versus the temperature are shown in Figures 7 and 8, respectively. $\chi_M T$ is equal to 15.4 (**1**) and 15.3 cm^3 mol^{-1} K (**2**) at room temperature. These values agree well with those expected for a Dy(III) (**1**) or Ho(III) (**2**) and four isolated Cu(II) ions ($\chi_M T = 14.14$ (Dy(III)) and 14.06 (Ho-

(24) Pei, Y.; Journaux, Y.; Kahn, O. *Inorg. Chem.* **1988**, *27*, 399.
(25) Benelli, C.; Caneschi, A.; Gatteschi, D.; Pardi, L.; Rey, P.; Shum, D. P.; Carlin, R. L. *Inorg. Chem.* **1989**, *28*, 272.
(26) Benelli, C.; Caneschi, A.; Gatteschi, D.; Pardi, L.; Rey, P. *Inorg. Chem.* **1990**, *29*, 4223.
(27) Benelli, C.; Caneschi, A.; Gatteschi, D.; Sessoli, R. *Inorg. Chem.* **1993**, *32*, 4797.
(28) Kahn, O.; Guillou, O. In *Research Frontiers in Magnetochemistry*; O'Connor, C. J. Ed.; World Scientific: Singapore, 1993; p 179.

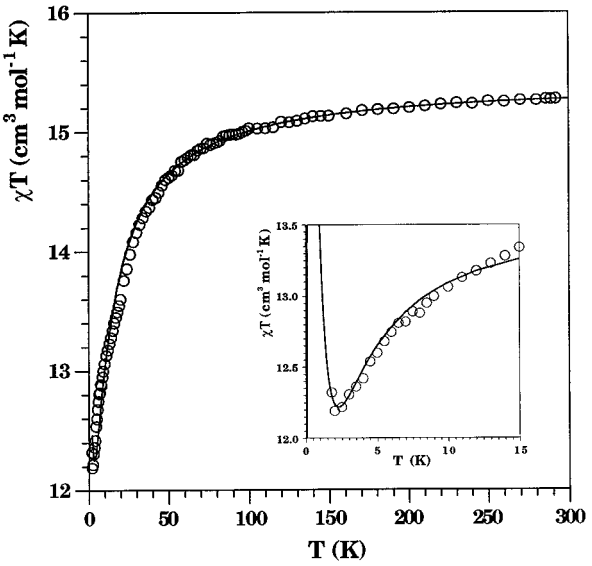

Figure 7. $\chi_M T$ versus T plot for complex **1**. The open circles are the experimental data, and the solid line corresponds to the theoretical fit through the Hamiltonian from eq 1. The inset shows the fit (solid line) in the low-temperature range using the Hamiltonian from eq 2 (see text).

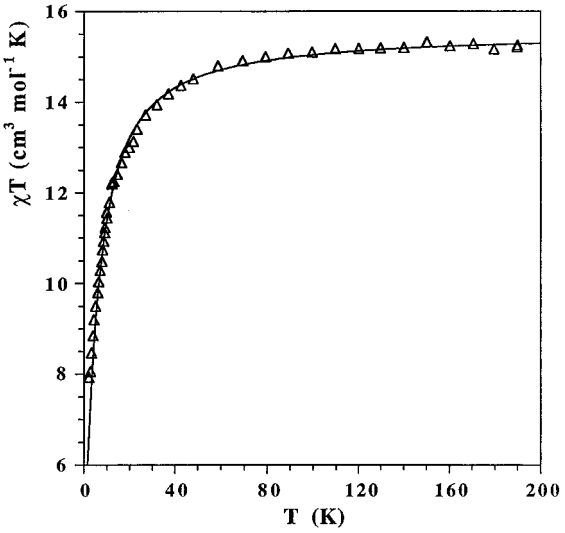

Figure 8. $\chi_M T$ versus T plot for complex **2**. The solid line corresponds to the theoretical fit through the Hamiltonian from eq 1 (see text).

(III)) $cm^3\ mol^{-1}\ K$ for the corresponding ground states $^6H_{15/2}$ ($g_{15/2} = 4/3$) and $^5I_8$ ($g_8 = 5/4$), respectively). The $\chi_M T$ values remain practically constant for both compounds down to 100 K, smoothly decrease as the temperature is lowered, and reach values equal to 12.3 (**1**) and 7.9 (**2**) $cm^3\ mol^{-1}\ K$ at 1.8 K.

In contrast to the Gd(III)−Cu(II) case, Dy(III) and Ho(III) have very large orbital moments. To our knowledge, there are only a few studies addressing this problem, and they are difficult to transfer to these molecular compounds for simulating quantitatively their magnetic properties.[29] In order to analyze the magnetic properties of **1** and **2**, as a first step we considered Ln(III) as free ions; that is, factors such as ligand field effects were neglected. In so doing, their magnetic properties can be interpreted through the isotropic Hamiltonian from expression 1, where S_{Gd} is substituted by the total angular momentum $J_{Dy} = 15/2$ or $J_{Ho} = 8$. The parameters obtained through a least-squares fit to this expression are as follows: $J_{DyCu} = -0.23\ cm^{-1}$, $J_{CuCu} = -2.7\ cm^{-1}$, $g_{Cu} = 2.09$, and $R = 9 \times 10^{-5}$; $J_{HoCu} = -0.36\ cm^{-1}$, $J_{CuCu} = -0.8\ cm^{-1}$, $g_{Cu} = 2.10$, and $R = 1.4 \times 10^{-4}$. The values of g_{Dy} and g_{Ho} were kept constant and were equal to 4/3 and 5/4, respectively. These parameters can reproduce the experimental susceptibility data in the whole range of temperatures, as shown in Figures 7 and 8. Although this approach could be appropriate in the high-temperature range, where the energy gaps induced by ligand-field effects are smaller than kT, at low temperatures, it should be inappropriate even if it fortuitously reproduces the experimental data. Consequently, the J values so obtained should be taken as the upper limit, because they would include ligand field effects such as a selective depopulation of the low-lying levels.

Owing to the fact that the shape of the curve is dominated by ligand field effects and to the occurrence of weak magnetic interactions, the question at hand is whether these spin interactions are antiferromagnetic or ferromagnetic. A clear-cut answer to this question involves a detailed analysis of the magnetic data in the low-temperature range. For that, we assumed that Dy(III) can be approximated to an effective spin $S_{eff} = 1/2$ with anisotropic g values. This is possible because an Ising-like behavior is frequently exhibited by Dy(III)-containing compounds.[30] In fact, EPR studies have shown that in general the values of $g_\perp$ are very small with respect to that of $g_{||}$, which is very large. This anisotropy of g allows the treatment of compound **1** as an Ising system at low temperatures. The $^6H_{15/2}$ ground state is split into a set of Kramers doublets, $|\pm M_{Jz}\rangle$. Thus, an anisotropic exchange model (eq 2) is expected to be

$$\hat{H}_{ex} = -\sum_{i=1}^{4} J^{||}_{DyCui}\hat{S}^z_{Dy}\hat{S}^z_{Cui} - \sum_{i=1}^{4} J^{\perp}_{DyCui}(\hat{S}^x_{Dy}\cdot\hat{S}^x_{Cui} + \hat{S}^y_{Dy}\cdot\hat{S}^y_{Cui}) - \sum_{j>i=1}^{4} J^{||}_{CuiCuj}\hat{S}^z_{Cui}\hat{S}^z_{Cuj} - \sum_{j>i=1}^{4} J^{\perp}_{CuiCuj}(\hat{S}^x_{Cui}\cdot\hat{S}^x_{Cuj} + \hat{S}^y_{Cui}\cdot\hat{S}^y_{Cuj}) \quad (2)$$

appropriate for the analysis of the magnetic properties of **1** at low temperatures, where it is assumed that only the ground-state Kramers doublet is populated.

The || and ⊥ symbols refer to the component parallel and perpendicular to the spin direction, and i and j denote to the Cu sites. In view of the whole symmetry of $Dy^{III}Cu^{II}_4$ (tetrahedral arrangement of Cu around central Dy) we can assume that the Cu sites are identical; $J_{DyCui} = J_{DyCuj}$ and $J_{CuiCuj} = J_{CuCu}$. In addition, an isotropic interaction between the Cu's, that is, $J^{||}_{CuCu} = J^{\perp}_{CuCu} = J_{CuCu}$ and $g^{||}_{Cu} = g^{\perp}_{Cu} = g_{Cu}$, was also assumed. These reasonable assumptions reduce the number of adjustable parameters in the fitting procedure. The following set of parameters is thus involved: $J^{||}_{DyCu}$, $J^{\perp}_{DyCu}$, J_{CuCu}, $g^{||}_{Dy}$, $g^{\perp}_{Dy}$, g_{Cu}.[22b] The fitting of the experimental susceptibility data is complicated by the fact that the J_{DyCu} (parallel and perpendicular components) and J_{CuCu} parameters are strongly correlated and a large series of values are possible. We fit the experimental data for **1** in the temperature range 1.8−15 K under the conditions that $J_{CuCu} < 0$ and $|J_{CuCu}| < 2\ cm^{-1}$. The best fit to the data under these conditions involves the following set of parameters: $J^{||}_{DyCu} = 3.4\ cm^{-1}$, $J^{\perp}_{DyCu} = -1.0\ cm^{-1}$, $J_{CuCu} = 0.9\ cm^{-1}$, $g^{||}_{Dy} = 14.1$, $g^{\perp}_{Dy} = 3.2$, and $g_{Cu} = 2.09$ ($R = 8 \times 10^{-5}$). The insert of Figure 7 shows the thermal dependence of the experimental $\chi_M T$ values in the low-temperature range as well as the theoretical curve using the above-quoted values.

(29) Levy, P. M. *Phys. Rev.* **1966**, *147*, 147.

(30) Carlin, R. L. *Magnetochemistry*; Springer-Verlag: Berlin, Heidelberg, New York, Tokyo, 1986.

It deserves to be pointed out that the fit, under the above conditions, leads always to $J^{\parallel} > 0$ and $J^{\perp} < 0$. The shape of the $\chi_M T$ curves as a function of $J^{\parallel}/J^{\perp}$ (α) ratio, with the other parameters kept constant, is shown in Figure 9. Our experimental data are clearly located in the region of negative values for α, the value of α being between -3 and -4 cm^{-1}, ruling out the possibility of $\alpha > 0$ except if physically meaningless values are allowed for J_{CuCu} ($J_{CuCu} > 0$ or $|J_{CuCu}| > 2$ cm^{-1}, for instance). Moreover, the occurrence of intermolecular interactions in Ln(III)-containing complexes where Ln(III) has a very large anisotropic magnetic moment, as in the present case, should be also considered. In this respect, it is well-known that for these salts they can be very important and dominate in the low-temperature region. However, the consideration of this intermolecular interaction in our expression introduces an overparameterization and leads to ambiguous values, because this interaction can be positive or negative in nature. In fact, this is the great problem because the Ln(III)−Cu(II) magnetic coupling in these systems is weak and can only be studied in the low-temperature region, where the dipolar interactions could play a key role.

In order to understand the meaning and consequences of the occurrence of a negative anisotropy ($\alpha < 0$, $J^{\parallel} > 0$, and $J^{\perp} < 0$), it is interesting to compare the zero-field (eq 3) and uniaxially symmetric (eqn 4) Hamiltonians. The Hamiltonian from eq 3

$$\hat{H} = -J\hat{S}_1 \cdot \hat{S}_2 - \hat{S}_1 D \hat{S}_2 \tag{3}$$

$$\hat{H} = -J^{\parallel}\hat{S}_{1z}\hat{S}_{2z} - J^{\perp}(\hat{S}_{1x}\hat{S}_{2x} + \hat{S}_{1y}\hat{S}_{2y}) \tag{4}$$

describes the interaction between two $S = 1/2$ centers, where J is a scalar which represents the isotropic part of the exchange interaction and D is a traceless tensor accounting for the anisotropic contribution (its effect is to split the triplet state). As far as the Hamiltoninan from eq 4 is concerned, it describes the exchange interaction between two anisotropic spins $S = 1/2$ (Dy ($S_{eff} = 1/2$) and Cu ($S = 1/2$)), where the exchange anisotropy is accounted for by considering the two effective exchange interactions $J^{\parallel}$ and $J^{\perp}$.

It can be readily shown[31] that when $D_{xx} = D_{yy}$ in the expression (3), both Hamiltonians (3) and (4) are equivalent and $J^{\parallel}$ and $J^{\perp}$ can be related to the parameters J and D from (3) through the expressions

$$J^{\parallel} = J + D_{zz} \tag{5}$$

$$J^{\perp} = J - D_{zz}/2 \tag{6}$$

where

$$J = {}^1/_3(J^{\parallel} + 2J^{\perp}) \tag{7}$$

$$D = {}^3/_2 D_{zz} \tag{8}$$

From eqs 5−8 and using the corresponding values for $J^{\parallel}$ and $J^{\perp}$ observed in **1**, we obtained $J \approx 0.5$ cm^{-1} and $D_{zz} \approx 3$ cm^{-1} ($D \approx 4.5$ cm^{-1}), revealing that the spin−spin interaction between Dy^{III} and Cu^{II} is weakly ferromagnetic and that D is larger than J ($\alpha < 0$ implies $D > 3J$). Therefore, D dominates the magnetic behavior in the $Dy^{III}-Cu^{II}$ interaction, precluding an accurate determination of the J value. This curious phenomenon is only possible when a weak magnetic coupling occurs (such as in the Ln(III)−Cu(II) systems) and a very large anisotropy is present (as for the extremely anisotropic Dy^{III} ion).

(31) de Jongh, L. J. In ref 23, p 1.

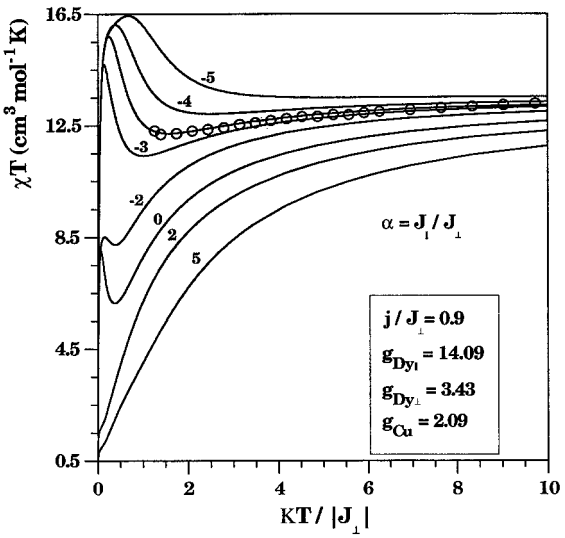

Figure 9. Thermal dependence of $\chi_M T$ as a function of α (open circles are the experimental data). $j = J_{CuCu}$.

As far as compound **2** is concerned, although the isotropic values of J_{HoCu} and J_{CuCu} obtained by a fit of $\chi_M T$ (*vide supra*) are reasonable, some doubts arise dealing even with the nature of the magnetic interaction as shown above for **1** (that is, the possibility of a ferromagnetic Ho(III)−Cu(II) interaction masked by ligand-field effects and/or intermolecular interactions). In order to analyze the experimental data of **2** in the low-temperature range, one should take into account that Ho(III) ($4f^{10}$) is a non-Kramers ion with a $^5I_8$ ground state which at low temperature can be treated as an Ising-like ion with $S_{eff} = 1$. However, this pseudo-triplet is generally split in the $|0\rangle$ and $|\pm 1\rangle$ components, i.e., a situation analogous to that of a Ni(II) ion ($S = 1$) with a zero-field splitting. The energy gap between $|0\rangle$ and $|\pm 1\rangle$ introduces an additional complication in the analysis on the nature of the Ho(III)−Cu(II) magnetic interaction. When this additional local anisotropy (which can be either positive or negative in nature) on the pseudo-triplet was taken into account (Hamiltonian (2)), we could not obtain a reliable set of parameters, analogous to what occurred on considering the intermolecular interactions in the $DyCu_4$ example.

These features make neccessary magnetic anisotropy measurements as well as EPR studies on single crystals of **2**. The growing of large single crystals which are needed to do that is the limiting step, and further efforts will be devoted to this aspect in the near future.

Conclusions. The main conclusions derived from the present work are as follows.

(i) The ferromagnetic coupling between Gd^{III} and Cu^{II} is again observed, and thus, it seems to be independent of the topology of the complex molecule (dimer, trimer, tetramer, pentamer, or chain).

(ii) The intramolecular $Cu^{II}-Cu^{II}$ magnetic coupling has to be considered in this kind of system. In this regard, the shape of the experimental magnetic curve showing global antiferromagnetic or Curie law behavior could not correspond to an $Gd^{III}-Cu^{II}$ antiferromagnetic coupling or no coupling between these ions, respectively.

(iii) The analysis of magnetic curves involving systems containing Ln^{III} cations with a large orbital contribution is very complicated. Even the use of an Ising approach to treat experimental data in the low-temperature range introduces overparameterization, and in addition, for these cases with high anisotropy, the zero-field splitting can be larger than the

magnetic interaction, making difficult an accurate determination of *J*. In order to obtain a reliable set of parameters, we have assumed that the Cu−Cu interactions are identical and isotropic, being negative and not larger than 2 cm^{-1}. Although these assumptions are reasonable, we have no idea on the temperature below the ground Kramers doublet is the only populated state as well as on the influence of the dipolar interactions in the low-temperature range. In our treatment, we assumed that the Kramers ground state is the only one populated at $T < 15$ K and that the dipolar interactions do not have a significant influence even at temperatures as low as 2 K. Under these assumptions, the $Dy^{III}-Cu^{II}$ magnetic coupling is found to be ferromagnetic as in the $Gd^{III}-Cu^{II}$ case.

(iv) Finally, in order to give a clear-cut answer to the ferromagnetic nature of the Ln(III)−Cu(II) coupling, the magnetic behavior of discrete and well-isolated Ln(III)−Cu(II) dimers should be investigated. These systems are the best candidatesto check this ferromagnetic coupling because of the lack of Cu−Cu and dipolar interactions.

Acknowledgment. This work was supported by by the Spanish DGICYT (Project PB94-1002), the French CNRS, the Spanish-French Integrated Actions and the Human Capital and Mobility Program (Network on Magnetic Molecular Materials from EEC) through Grant ERBCHRX-CT920080. R.R. also thanks the Spanish Ministry of Science and Education for a postdoctoral fellowship.

Supporting Information Available: Tables giving crystal data, anisotropic thermal parameters, hydrogen atom coordinates, and intramolecular bond distances and angles for **1** and **2**, two drawings showing the overlap between two Ln[Cu(apox)] entities (Ln = Dy (**1**), Ho (**2**)), and Appendices A and B (17 pages). Ordering information is given on any current masthead page.

IC960524T